Atmos. Chem. Phys. Discuss., https://doi.org/10.5194/acp-2019-18
Manuscript under review for journal Atmos. Chem. Phys.
Discussion started: 28 January 2019

Atmospheric Chemistry and Physics Discussions

Observationally constrained analysis of sea salt aerosol in the marine atmosphere

Huisheng Bian[1,2], Karl Froyd[3,4], Daniel M. Murphy[3], Jack Dibb[5], Mian Chin[2], Peter R. Colarco[2], Anton Darmenov[2], Arlindo da Silva[2], Tom L. Kucsera[6], Gregory Schill[3,4], Hongbin Yu[2], Paul Bui[7], Maximilian Dollner[8], Bernadett Weinzierl[8], and Alexander Smirnov[9]

[1] University of Maryland at Baltimore County, Baltimore County, MD

[2] NASA Goddard Space Flight Center, Greenbelt, MD

[3] NOAA Earth System Research Laboratory, Chemical Sciences Division, CO

[4] Cooperative Institute for Research in Environmental Sciences, University of Colorado, Boulder, CO

[5] University of New Hampshire, Durham, NH

[6] Universities Space Research Association, Columbia, MD

7 NASA Ames Research Center, Moffett Field, CA

8 University of Vienna, Faculty of Physics, Aerosol and Environmental Physics , Boltzmanngasse 5, A-1090 Wien, Austria

9 Science Systems and Applications, Inc., Lanham, MD 20706

Abstract

Atmospheric sea salt plays important roles in marine cloud formation and atmospheric chemistry. We performed an integrated analysis of NASA GEOS model simulations run with the GOCART aerosol module, in situ measurements from the PALMS and SAGA instruments obtained during the NASA ATom campaign, and aerosol optical depth (AOD) measurements from AERONET Marine Aerosol Network (MAN) sun photometers and from MODIS satellite observations to better constrain sea salt in the marine atmosphere. ATom measurements and GEOS model simulation both show that

Atmos. Chem. Phys. Discuss., https://doi.org/10.5194/acp-2019-18
Manuscript under review for journal Atmos. Chem. Phys.
Discussion started: 28 January 2019

Atmospheric Chemistry and Physics Discussions

sea salt concentrations over the Pacific and Atlantic oceans have a strong vertical gradient, varying up to four orders of magnitude from the marine boundary layer to free troposphere. The modeled residence times suggest that the lifetime of sea salt particles with dry diameter less than 3 μm is largely controlled by wet removal, followed next by turbulent process. During both boreal summer and winter, the GEOS simulated sea salt mass mixing ratios agree with SAGA measurements in the marine boundary layer (MBL) and with PALMS measurements above the MBL. However, comparison of AOD from GEOS with AERONET/MAN and MODIS aerosol retrievals indicated that the model underestimated AOD over the oceans where sea salt dominates. The apparent discrepancy of slightly overpredicted concentration and large underpredicted AOD could not be explained by biases in the model RH, which was found to be comparable to or larger than the in-situ measurements. This conundrum is at least partially explained by the sea salt size distribution; where the GEOS simulation has much less sea salt percentage-wise in the smaller particles than was observed by PALMS. Model sensitivity experiments indicated that the simulated sea salt is better correlated with measurements when the sea salt emission is calculated based on the friction velocity and with consideration of sea surface temperature dependence than that parameterized with the 10-m winds.

1. Introduction

Bubble bursting and jet drops at the ocean surface result in the production of sea spray particles composed of inorganic sea salt and organic matter (e.g., Quinn and Bates, 2013). Among various atmospheric aerosol components, sea salt is estimated to have the largest

Atmos. Chem. Phys. Discuss., https://doi.org/10.5194/acp-2019-18
Manuscript under review for journal Atmos. Chem. Phys.
Discussion started: 28 January 2019

Atmospheric Chemistry and Physics Discussions

mass emission flux and the second largest atmospheric mass loading globally (Textor et al., 2006). Sea salt particles in the atmosphere could exert direct radiative effect of around -1.5 to -5.03 W/m^2 annually at the top of atmosphere (IPCC, 2001). On a global and annual scale, the direct radiative effect of sea salt is equal to or greater in magnitude than that of natural sulfate and soil dust (Jacobson, 2001; Takemura et al., 2002). Sea salt particles are efficient cloud condensation nuclei (CCN). Consequently, sea salt particles have indirect effects on climate and weather (Dadashazaer et al., 2017; Dall et al., 2017; Kogan et al., 2012; Pierce and Adams, 2006; Quinn et al., 2017). Furthermore, sea salt aerosol particles serve as sinks for reactive gases and small particles and are a source of halogens to the atmosphere (e.g., Alexander al., 2005; Anastasio et al., 2007; Lawlet et al., 2011). There is also observational evidence suggesting that new particle formation may be suppressed in the presence of sea salt aerosol (Browse et al., 2014; Lewis and Schwartz, 2004). To quantify the effects of sea salt aerosol on the environment, a detailed knowledge of its mass, size, and vertical distribution is required.

We present a comprehensive evaluation of sea salt aerosol simulated with the Goddard Chemistry, Aerosol, Radiation, and Transport model (GOCART) in the Goddard Earth Observing System (GEOS) framework using aerosol measurements obtained during the Atmospheric Tomography Mission (ATom). ATom is a NASA-funded Earth Venture-suborbital project. ATom deployed an extensive gas and aerosol instrumental payload on the NASA DC-8 aircraft for systematic, global-scale sampling of the atmosphere, profiling continuously from 0.2 to 12 km altitude with flight routes over the Pacific, Atlantic, Southern Ocean, North America and Greenland from 85°N to 65°S (see Fig. 1).

Atmos. Chem. Phys. Discuss., https://doi.org/10.5194/acp-2019-18
Manuscript under review for journal Atmos. Chem. Phys.
Discussion started: 28 January 2019

Atmospheric Chemistry and Physics Discussions

Flights occurred in four seasons over a 3-year period (2016-2018) and we study the first two ATom measurements that represent the summer and winter seasons for both hemispheres. The ATom data provides an unprecedented opportunity for models to evaluate transport and parameterizations of physical and chemical processes. This work utilizes ATom's high frequency vertical measurements of sea salt over global remote oceans from marine boundary layer (MBL) to the upper troposphere, in contrast with typical model validation of sea salt simulation with in situ measurements at ground surface limited to selected locations and regions (Kishcha et al., 2011; Spada et al., 2013, 2015; Tsyro et al., 2011; Witek et al., 2007), and commonly using monthly averaged observations (Grini et al., 2002; Textor et al., 2006).

In this study, we examine sea salt in MBL using both the ATom measurements and GEOS GOCART simulations. We explore sea salt vertical distribution in various latitudinal zones over the Pacific and Atlantic oceans to investigate simulated dry and wet deposition processes. Finally, we examine the sea salt size distribution, important to both AOD calculations and cloud formation.

The GEOS/GOCART model is described in section 2, particularly the different sea salt emission schemes tested in this study. The NASA ATom field campaign is introduced in section 3, including a brief description of the Particle Analysis by Laser Mass Spectrometry (PALMS) and Soluble Acidic Gases and Aerosols (SAGA) instruments that are used to provide sea salt measurements. The measurements and model results are presented in section 4 and the emission, removal processes, vertical profile, size

Atmos. Chem. Phys. Discuss., https://doi.org/10.5194/acp-2019-18
Manuscript under review for journal Atmos. Chem. Phys.
Discussion started: 28 January 2019

Atmospheric Chemistry and Physics Discussions

distributions, and AOD are analyzed. In section 5, we summarize our sea salt study and discuss the potential important chemical/physical processes that could have an impact on sea salt simulation for future improvement.

2. Model description

Global sea salt is simulated by using GEOS/GOCART, which is a global aerosol model GOCART (Chin et al., 2002, 2009, 2014) implemented in the GEOS Earth system model (Gelaro et al., 2017; Rienecker et al., 2011). The GEOS/GOCART aerosols include dust, sea salt, sulfate, nitrate, ammonium, black carbon, and organic matter, mixed externally (Bian et al., 2013; 2017; Colarco et al., 2010).

The sea salt emission scheme in the GEOS/GOCART model was initially based on the algorithm of Gong (2003) who provided a parameterization of the size-resolved flux of sea salt particles as a function of the 10-m wind speed. Two modifications to this scheme were subsequently developed based on comparisons of simulated sea salt aerosol to satellite AOD from the Moderate Resolution Imaging Spectroradiometer (MODIS) (Darmenov et al., 2013; Randles et al., 2017): 1) the emission function was recalibrated in terms of the surface friction velocity rather than the 10-m wind speed and 2) a sea surface temperature (SST) correction term was introduced. This new emission algorithm with both surface wind and temperature modifications is used in the main body of the paper and a detailed description of the emission is given in supplementary material. We examined the three sea salt emission schemes using ATom measurements and the results are given in supplementary material.

Atmos. Chem. Phys. Discuss., https://doi.org/10.5194/acp-2019-18
Manuscript under review for journal Atmos. Chem. Phys.
Discussion started: 28 January 2019

120

121 The current default setting of GEOS/GOCART allows sea salt to be completely removed
122 by warm clouds from convective updraft and from large-scale rainout and washout. Sea
123 salt can also be removed by dry deposition (turbulent) and sedimentation. These
124 processes were described in Chin et al. (2002). We assume that the particles undergo
125 hygroscopic growth according to the equilibrium parameterization of Gerber (1985),
126 which is a function of the relative humidity (RH). The humidified particle sizes are
127 considered in our computations of the particle sedimentation, aerodynamic deposition
128 velocity, and optical properties.

129

130 The GEOS/GOCART includes five bulk sea salt size bins in the range of 0.06-20 μm in
131 dry diameter. Specifically, they are 0.06-0.2, 0.2-1.0, 1.0-3.0, 3.0-10, and 10-20 μm,
132 respectively. The first bin was added to facilitate aerosol-cloud and optical property
133 studies (Colarco et al. 2010), which was not included in the previous GOCART versions
134 (Chin et al., 2002, 2014). The sea salt particle density is 2200 (kg/m^3) for all sizes.

135

136 In this study, we ran GEOS/GOCART at a global ~50 km horizontal resolution on the
137 cubed-sphere grid and 72 vertical layers from surface up to 0.01mb. We ran the model in
138 "replay" mode, which sets the model dynamical state (winds, pressure, and temperature)
139 at every 6 hours to the balanced state provided by the meteorological reanalysis fields
140 from the Modern-Era Reanalysis for Research and Applications version 2 (MERRA-2).
141 One and half year simulation was conducted from the beginning of 2016 to cover the first

Atmos. Chem. Phys. Discuss., https://doi.org/10.5194/acp-2019-18
Manuscript under review for journal Atmos. Chem. Phys.
Discussion started: 28 January 2019

two phases of ATom measurement periods, with the first half year of the simulation used as a spin up period.

3. ATom aircraft sea salt measurement from PALMS and SAGA

ATom provides measurements for various important atmospheric gases, aerosols and their precursors over vast open oceans. Among these, sea salt has been measured by two instruments, the NOAA PALMS instrument, which provides mass mixing ratio and size distribution up to 3 μm in dry diameter, and the University of New Hampshire SAGA instrument, which includes measurements of sodium ion, a good sea salt proxy.

PALMS is a laser ionization mass spectrometer which makes in situ measurements of the chemical composition of individual aerosol particles. A detailed description of PALMS, including its physical working mechanism and measurement features, has been given by Murphy et al., (2018). The instrument is capable of measuring particles from 0.12 to 3 μm in dry diameter and analysis is completed in less than 1 millisecond after the aerosols enter the inlet. The real power of the PALMS sea salt measurements is twofold: a) high sensitivity at low concentrations above the MBL such that the measured vertical profiles are more reliable than most previous data, and b) the data are size-segregated up to 3 μm in dry diameter, covering the active size range for optical and radiation calculations.

In the cloud-free MBL, sea salt concentrations inferred from the SAGA sodium data are highly correlated with PALMS sea salt measurements (Murphy et al., 2018). SAGA measures sodium ions extracted from the aerosol. A factor of 3.27 is applied to convert the SAGA measured sodium mass to total sea salt mass (Keene et al., 1986; Wilson,

1975). This assumes that all of the measured sodium comes from sea salt, which should be a reasonable assumption for most ATom samples. SAGA collects particles on a filter with a sampling frequency of around 5-15 minutes to allow more time for the filter media to collect sufficient particles. As reported by the DC-8 Inlet Characterization Experiment (DICE), the SAGA inlet performed nearly identically in the marine boundary environment to the U. Hawaii inlet used by PALMS during ATom (McNaughton et al., 2007).

We use ATom1 (Jul.-Aug., 2016) and ATom2 (Jan.-Feb., 2017) campaign data in this study. These two deployments combined together provided detail information of summer and winter on a global scale.

4. Results and Discussions

4.1 Comparison in marine boundary layer

Sea salt is sufficiently rich in the MBL that SAGA can collect enough aerosol there for analysis. Comparisons of the sea salt in a layer from surface up to 1.5 km between the model simulation and ATom (PALMS and SAGA) measurements are shown in Fig. 2a. To have a reasonable comparison, we conducted three data treatments. First, we excluded SAGA samples with significant dust signal when the measurements meet the two conditions: sample Ca^{2+} larger than 0.05 μg/sm^3 and the ratio of Ca^{2+} to Na^{+} larger than 0.06. Second, we only include GEOS sea salt particles smaller than 3 μm in dry diameter to be consistent with the instrument measurements. Third, we sampled GEOS and

Atmos. Chem. Phys. Discuss., https://doi.org/10.5194/acp-2019-18
Manuscript under review for journal Atmos. Chem. Phys.
Discussion started: 28 January 2019

Atmospheric Chemistry and Physics Discussions

PALMS data at the SAGA measurement time frequency when the SAGA has valid measurements. The agreement between model and measurement is good. The correlation coefficients are generally higher than 0.79 for both GEOS-PALMS and GEOS-SAGA in both ATom1 and 2 periods.

There are outliers on the Figure 2a. Just a small amount of cloud can wash off salt previously deposited on an inlet wall. Therefore, in Figure 2b we excluded samples that could be contaminated by clouds during sampling, using cloud indicator data from the Cloud, Aerosol, and Precipitation Spectrometer (CAPS). The outliers are gone on Figure 2b and the correlation coefficients between model and measurements are indeed improved a little bit, i.e. larger than 0.85. On the other hand, the GEOS sea salt mass mixing ratios are still more than double of those of PALMS (2.3 in ATom1 and 4.7 in ATom2), which could be at least partially explained by potential sampling biases in PALMS instrument, particularly in the size distribution. The cutpoint of 3 μm in dry diameter recommended by instrument teams used in this study is subject to a large uncertainty of wet/dry size ratio that is strongly dependent on ambient relative humidity. Furthermore, the sea salt mass distribution is (sometimes) still rising sharply through the inlet cutpoints. Considering the combination of all these systematic and random uncertainties, which are decreased across the sea salt coarse mode, the measurement can easily result in uncertainties on the order of ~x2 in dry mass. When checking the comparison between GEOS and SAGA, GEOS sea salt mixing ratio is comparable to or slightly larger than SAGA results (i.e. 0.92 in ATom1 and 1.3 in ATom2). Overall, the GEOS sea salt is most likely to overestimate sea salt mass during southern hemisphere

summer period. Comparing sea salt between the two instruments directly shows a high correlation (0.76 in ATom1 and 0.90 in ATom2) as well (also see Murphy et al., 2018).

4.2 Vertical distribution

Understanding the sea salt vertical distribution is important for climate studies, particularly in the tropical marine upper troposphere where a reliable background aerosol field is needed. However, most previous sea salt measurements were limited to the surface or near coastal areas, leading to nearly no in situ observations of the vertical distribution of sea salt over vast areas of the open oceans. The ATom measurements fill this gap by providing atmospheric tomography measurements over the Pacific, Atlantic, and Southern oceans from near surface to the upper troposphere (0.2-12 km). Furthermore, the PALMS instrument measures in situ sea salt mass and size distribution. A good sensitivity of the PALMS measurements makes it very useful in studying the relatively clean environments above the MBL. Using the ATom sea salt measurements over remote open oceans has some additional advantages versus previous studies. For instance, airborne measurements alleviate biases typical at land stations due to onshore wave breaking activities, especially at sites with steep topography (Witek et al., 2007; Spada et al., 2015).

Figure 3 shows the sea salt vertical profiles of PALMS measurement and GEOS model simulation over 5 latitudinal zones over Pacific and Atlantic oceans in ATom1 and ATom2. The GEOS model results are sampled at the time and location closest to the measurement points. As discussed in section 4.1, modeled sea salt mass concentrations

are higher than the PALMS data near the surface over all latitudinal zones during both summer and winter seasons. There are often two regimes vertically with a sharp gradient in the lower atmosphere and a lesser gradient above. Wet removal processes, particularly convective cloud removal, are likely the driving factors for the sea salt distribution in the size range considered in this study (Table 1a). Sea salt is a highly soluble species. It is assumed to fully dissolve into clouds, which results in efficient removal by shallow marine clouds, typically marine stratus and stratocumulus clouds (Eastman et al., 2011, Lebsock et al., 2011, Wood 2012, Zhou et al., 2015). Sea salt dry deposition (turbulent) and sedimentation also contribute to its removal in low altitudes. Interestingly, sedimentation process plays the smallest removal role for the sea salt particles studied in this work, while it overwhelmingly controls sea salt loss rate (i.e. more than 1.5 times those of all other processes combined) when coarser mode sea salt is included, see Table 1b. This is understandable because nearly 90% of injected sea salt particles are in coarse mode. Since sea salt is found mostly in the lower atmosphere, further removal of sea salt particles by cold clouds was found to have only marginal impact on its mass budget in our sensitivity studies, although its feedback on cold clouds needs further studies. Note that results in Table 1a and b are summarized on an annual basis from July 2016 to June 2017.

Atmospheric convection impacts the sea salt vertical distribution as well. The height of the turnaround level (or the transition layer) between two vertical distribution regimes in Fig. 3 is around 600 hPa in the polar regions and moves up to 400 hPa in the tropical region, given that more vigorous convective activities occur in the tropical region. The

256 seasonal variation of the vertical gradient is larger in polar regions than in tropical region,
257 consistent with stronger seasonal variations of the meteorological fields (e.g. T, RH,
258 wind, etc) in high latitudes.
259
260 **4.3 Marine aerosol AOD**
261 To provide an overall picture of sea salt for this study, we compared the GEOS AOD
262 with satellite MODIS Collection 6 (C6) Aerosol AOD retrieval (Levy et al., 2013) and
263 AERONET Maritime Aerosol Network (MAN) measurements (Smirnov et al., 2017) by
264 focusing on sea salt dominant regions. AOD integrates extinction by all aerosol in the
265 atmospheric column, with extinction dependent on the absolute mass, size distribution,
266 hygroscopic growth, vertical distribution, and optical property of each individual
267 component and the composition of aerosols.
268
269 Figure 4 shows total AOD comparison between MODIS and GEOS in August 2016 and
270 February 2017. Here, the GEOS AODs are sampled using daily MODIS AOD retrieval.
271 The AODs are only shown where the fraction of sea salt mass relative to the total aerosol
272 mass simulated by GEOS (bottom panel) is larger than 0.7 so that we can focus our
273 discussion over sea salt dominant regions. GEOS AODs are much lower than MODIS
274 AODs for both seasons over remote oceans where sea salt dominates. Even after
275 improvements, MODIS C6 AOD remains a positive bias up to 0.03 at low AOD (Figure
276 16 in Levy et al., 2013). It is difficult for us to remove this bias in the comparison shown
277 in the Figure 4. Another AOD comparison between AERONET MAN and GEOS,

278 therefore, is explored since there is no positive systematic bias reported in MAN's
279 measurement.
280
281 The conclusion of a lower GEOS AOD can also be obtained in Fig. 5 by comparing AOD
282 between the MAN cruise measurement and the GEOS simulation that occurred from July,
283 2016 to June 2017. AERONET MAN provides ship-borne aerosol optical depth
284 measurements from the Microtops II sun photometers. The GEOS model results are
285 sampled at the time and location of the ship-based measurements. The model AODs are
286 much smaller than MAN measurements over a majority of the open ocean areas except
287 part of the Atlantic Ocean where AOD was impacted by the dust. The scatter plot at the
288 bottom of the figure indicates clearly that the modeled AOD is biased low, especially
289 over the Southern Ocean where the model AOD is less than half of MAN's.
290
291 On the one hand, GEOS' sea salt mass is comparable to SAGA *in situ* measurements in
292 the MBL, and on the other hand, GEOS underestimates AOD when compared with
293 measurements from MAN and MODIS. The agreement with PALMS vertical gradients
294 shows that the AOD cannot be explained by sea salt above the MBL. There are various
295 potential reasons for this conundrum, such as the sea salt size distribution, atmospheric
296 relative humidity, sea salt particle hygroscopic growth rate, sea salt refractive index, etc.
297 We will discuss the first two potential reasons below.
298
299 **4.4 Size distribution and atmospheric RH**

Atmos. Chem. Phys. Discuss., https://doi.org/10.5194/acp-2019-18
Manuscript under review for journal Atmos. Chem. Phys.
Discussion started: 28 January 2019

The sea salt size distribution is a key factor in AOD calculation because small particles are more optically efficient. Sea salt size distribution also affects AOD calculation by affecting sea salt mass distribution via sea salt transport and removal processes. The necessity to study sea salt size distribution lies also in that it plays an important role in atmospheric chemistry, radiative effects, and cloud formation processes.

To quantify size impact, we calculate normalized percentage of sea salt mass in each of the first three size bins for PALMS and GEOS over three atmospheric vertical layers for ATom1 and 2, as shown in Figure 6. The three vertical layers (i.e. 0-1.5, 1.5-6, and >6 km) represent the boundary layer, middle troposphere, and upper troposphere. GEOS sea salt particle mass and size have been computed at RH of 45% to match the measurement condition of PALMS. Although the particle sizes are limited to be less than 3 μm in dry diameter here due to PALMS measurements, we are more interested in the small particles since they are optically important and are more important in cloud formation on a per unit mass basis. The amplitude of the distribution is much shallower in PALMS than in GEOS. In other words, with the same sea salt mass, the fraction of sea salt in the finest mode in PALMS would be much more (i.e. about 5-7 times higher) than in GEOS. To quantify the potential impact of sea salt size distribution on AOD calculation, we calculate the sea salt mass extinction efficient (MEE) integrated over the three bins using the two size distributions of PALMS and GEOS at RH 45% and 550 nm in the same three vertical layers and in the whole atmosphere (Table 2). The size segregated MEEs used in the calculation are 1610.3618, 5622.7075, and 1216.4149 m^2 kg^{-1} for the bins 1-3, respectively. The integrated MEE of GEOS (1679.36 m^2 kg^{-1}) is only 76.2% of that of

PALMS (2203.67 m^2 kg^{-1}). Thus, the underestimation of GEOS AOD shown in Figure 5c is partially stemmed from the sea salt size distribution. The underestimation of AOD by GEOS is more significant in low atmosphere shown in Table 2, which implies that the sea salt size distribution from emission may need to be revisited.

Apparently, sea salt size distribution is a potential culprit for the dichotomy in GEOS simulation since GEOS partitions more sea salt onto larger particles which are less optically active compared with the significant fine sea salt mode observed in PALMS measurements. Such large underestimation of fine sea salt particles by the model may have significant implications not only on the AOD calculation but also on studies of radiative effects and cloud formation because particle number concentration is a key quantity for these processes. The conclusion that GEOS sea salt size distribution favors the coarse mode sea salt particles is consistent with a recent study of Naumann et al., (2016), which found that the sea salt emission of Gong (2003) yielded overestimations in the PM10 measured at coastal stations and underestimations at inland stations over northwestern Europe.

Sea salt particle size distribution changes horizontally and vertically, but the change is much smaller than the difference between those of model and measurement. This implies a possibility of using a global size distribution without sacrificing much accuracy.

Atmospheric water, another possible reason for the AOD underestimation, was also investigated. Figure 7 compares atmospheric RHs between ATom measurements and

GEOS simulations along flight tracks summarized over the same regions as in Fig. 3. Almost everywhere the model's RH is higher than ATom measurement, including MBL where humidity is typically high, with only a few exceptions. Thus, atmospheric water simulation is not responsible for the low AOD calculation. In fact, using measured RH along with the model's sea salt size distribution and vertical distribution would give even lower AOD. There should be other factors contributing to a lower GEOS AOD calculation as well, such as sea salt hygroscopic growth rate, sea salt optical properties, and other aerosol species over ocean. Further investigations for these factors are needed to better understand the GEOS sea salt simulation.

5. Conclusions

A systematic and comprehensive global sea salt study was conducted by integrating NASA GEOS model simulations with ATom in situ measurements from the PALMS and SAGA instruments, as well as AOD measurements from AERONET MAN and satellite MODIS over the oceans. This work takes advantage of PALMS sea salt vertical profile measurement together with SAGA filter measurements in MBL. The study covers global remote regions over the Pacific, Atlantic, and Southern Oceans from near the surface to ~12 km altitude and covers both summer and winter seasons. Important atmospheric sea salt fields, e.g. mass mixing ratio, vertical distribution, size distribution, and aerosol AOD, are examined. The meteorological field of RH and the sea salt simulation processes of emission, dry deposition, sedimentation, and large scale and convective wet depositions were explored to explain the sea salt fields and to reveal a potential direction for model improvement.

369

370 Generally, the agreement between ATom measurements and the model is remarkable,
371 both in terms of absolute loading and especially in the shape of the vertical distribution
372 under a huge variety of tropospheric environments. The correlation coefficients are
373 generally higher than 0.8 between GEOS-PALMS and GEOS-SAGA for both ATom1
374 and ATom2 periods. GEOS results captured the strong sea salt vertical gradient shown in
375 the measurements except over SH high latitudes, where the PALMS's gradient is deeper.
376 In the MBL, the current GEOS sea salt simulation is comparable (ATom1) or slightly
377 higher (ATom2) than SAGA data, which in turn is higher than PALMS data.

378

379 An underestimation of GEOS aerosol AOD over sea salt dominated oceans was found
380 from the comparison of AODs between GEOS and MAN, as well as GEOS and MODIS.
381 This is contradictory to the finding that GEOS sea salt mass abundance is comparable to
382 or slightly higher than measurements. This conundrum may be partially resolved by the
383 sea salt mass size distributions compared between GEOS and PALMS. The GEOS sea
384 salt mass size distribution favors the coarse mode while PALMS has a larger fraction of
385 more optically active submicron sea salt. The atmospheric water field, however, can be
386 ruled out as the cause of model underestimation of AOD, since the GEOS RH is
387 comparable to or higher than ATom measurements almost everywhere along the flight
388 tracks, especially in MBL.

389

390 Atmospheric sea salt vertical distribution is impacted by various processes including
391 emission, hygroscopic growth, dry deposition, sedimentation, wet deposition, convection,

and large-scale advection. Among these processes, wet deposition, owing to both shallow marine cloud structure and rapid hygroscopic growth of sea salt particles, is most important in shaping the vertical profile for the size range studied in this work and results in a sharp gradient in the low atmosphere where RH is typically very high. Vertical convection is also important.

More work is needed in the future to investigate sea salt hygroscopic growth rate, optical properties, sea water salinity, sea ice, and marine organic aerosol to understand the dilemma in GEOS simulation. Sea water salinity, which is missing in the GEOS aerosol model, has an impact not only on sea spray emission but also on sea spray aerosol (SSA) size. Barthel et al. (2014) reported that the dry SSA size distribution shifts towards smaller sizes with lower salinities found in the EMEP intensive campaigns. Sea ice, whose contribution is also missed in the GEOS aerosol model, could be an important source of sea salt aerosol over polar regions and has significant implications for polar climate and atmospheric chemistry reported by recent publications (Dall et al., 2017; May et al., 2016; Rhodes et al., 2017). More importantly, primary marine organic aerosols (Randles et al., 2004), which come also from sea spray bubble bursting as sea salts but are more submicron particles, should be investigated to disentangle the sea spray aerosols.

Author contribution

Huisheng Bian and Mian Chin designed the experiments. Peter R. Colarco, Anton Darmenov, Arlindo da Silva, Tom L. Kucsera, and Hongbin Yu contributed to GEOS-GOCART model setup and provided tools to analyze model data. Huisheng Bian conducted the model simulation and in

charge of the analyses. Karl Froyd, Daniel M. Murphy, and Gregory Schill provided ATom PALMS measurement data. Jack Dibb provided ATom SAGA measurement data. Maximilian Dollner and Bernadett Weinzierl provided ATom CAPS cloud data. Paul Bui provided ATom MMS data for RH measurement. Hongbin Yu and Alexander Smirnov provided MODIS satellite and AERONET MAN measurement data. All authors contributed to the data analyses and paper writing.

Acknowledgments

This research was support by two programs of the National Aeronautics and Space Administration (NASA): Atmospheric Composition: Modeling and Analysis Program (ACMAP) and Earth Venture-suborbital program for the Atmospheric Tomography Mission (ATom).

References:

Alexander, B., R. J. Park, D. J. Jacob, Q. B. Li, R. M. Yantosca, J. Savarino, C. C. W. Lee, and M. H. Thiemens (2005), Sulfate formation in sea-salt aerosols: Constraints from oxygen i sotopes, J. Geophys. Res., 110, D10307, doi:10.1029/2004JD005659.

Anastasio, C. and Newberg, J. T.: Sources and sinks of hydroxyl radical in sea-salt particles, J. Geophys. Res., 112, D10306, doi:10.1029/2006JD008061, 2007.

Barthel, S., Tegen, I., Wolke, R., and van Pinxteren, M.: Model study on the dependence of primary marine aerosol emission on the sea surface temperature, Atmos. Chem. Phys. Discuss., 14, 377-434, https://doi.org/10.5194/acpd-14-377-2014, 2014.

441 Bian, H., Chin, M., Hauglustaine, D. A., Schulz, M., Myhre, G., Bauer, S. E., Lund, M. T.,
442 Karydis, V. A., Kucsera, T. L., Pan, X., Pozzer, A., Skeie, R. B., Steenrod, S. D., Sudo, K.,
443 Tsigaridis, K., Tsimpidi, A. P., and Tsyro, S. G.: Investigation of global nitrate from the
444 AeroCom Phase III experiment, Atmos. Chem. Phys., 17, 12911-12940,
445 https://doi.org/10.5194/acp-17-12911-2017, 2017.
446 Bian, H., P. Colarco, M. Chin, G. Chen, J.M. Rodriguez, Q. Liang, et al., Investigation of source
447 attributions of pollution to the Western Arctic during the NASA ARCTAS field campaign.
448 Atmos. Chem. and Phys., 13, 4707-4721, doi:10.5194/acp-13-4707-2013, 2013.
449 Browse, J., Carslaw, K. S., Mann, G. W., Birch, C. E., Arnold, S. R., and Leck, C.: The complex
450 response of Arctic aerosol to sea-ice retreat, Atmos. Chem. Phys., 14, 7543-7557,
451 https://doi.org/10.5194/acp-14-7543-2014, 2014.
452 Chin, M., T. Diehl, Q. Tian, J. M. Prospero, R. A. Kahn, A. Remer, H. Yu, A. M. Sayer, H. Bian,
453 et al., Multi-decadal variations of atmospheric aerosols from 1980 to 2009: sources and
454 regional trends, Atmos. Chem. Phys., 14, 3657-3690, doi:10.5194/acp-14-3657-2014, 2014.
455 Chin, M., P. Ginoux, S. Kinne, B. N. Holben, B. N. Duncan, R. V. Martin, J. A. Logan, A.
456 Higurashi, and T. Nakajima, 2002: Tropospheric aerosol optical thickness from the
457 GOCART model and comparisons with satellite and sun photometer measurements, J.
458 Atmos. Sci. 59, 461-483.
459 Colarco, P., da Silva, A., Chin, M., and Diehl, T.: On- line simulations of global aerosol
460 distributions in the NASA GEOS-4 model and comparisons to satellite and ground based
461 aerosol optical depth, J. Geophys. Res., 115, D14207, doi:10.1029/2009JD012820, 2010.
462 Dadashazar, H., Wang, Z., Crosbie, E., Brunke, M., Zeng, X., Jonsson, H., Woods, R. K., Flagan,
463 R. C., Seinfeld, J. H., and Sorooshian, A.: Relationships between giant sea salt particles and
464 clouds inferred from aircraft physico-chemical data, J. Geophys. Res.-Atmos., 122, 3421–
465 3434, https://doi.org/10.1002/2016JD026019, 2017.

466 Dall'Osto, M., et al., Arctic sea ice melt leads to atmospheric new particle formation, Sci. Rep., 7
467 (1) (2017), p. 3318, 10.1038/s41598-017-03328-1.
468 Eastman, R., S. G. Warren, and C. J. Hahn, 2011: Variations in cloud cover and cloud types over
469 the ocean from surface observations, 1954–2008. J. Climate, 24, 5914–5934.
470 Gelaro, R., McCarty, W., Suárez, M. J., Todling, R., Molod, A., Takacs, L., Randles, C. A.,
471 Darmenov, A., Bosilovich, M. G., Reichle, R., Wargan, K., Coy, L., Cullather, R., Draper,
472 C., Akella, S., Buchard, V., Conaty, A., da Silva, A. M., Gu, W., Kim, G. K., Koster, R.,
473 Lucchesi, R., Merkova, D., Nielsen, J. E., Partyka, G., Pawson, S., Putman, W., Rienecker,
474 M., Schubert, S. D., Sienkiewicz, M., and Zhao, B.: The Modern-Era Retrospective Analysis
475 for Research and Applications, Version 2 (MERRA-2), J. Climate, 30, 5419–5454,
476 https://doi.org/10.1175/JCLI-D-16-0758.1, 2017.
477 Gerber, H. E. (1985), Relative-humidity parameterization of the Navy aerosol model (NAM),
478 NRL Rep. 8956, Naval Res. Lab., Washington, D. C.
479 Gong, S. L., A parameterization of sea-salt aerosol source function for sub- and super-micron
480 particles, Global Biogeochem. Cycles, 17 (4), 1097, doi:10.1029/2003GB002079, 2003.
481 Intergovernmental Panel on Climate Change (IPCC) 2001 In Climate Change 2001: The
482 Scientific Basis (eds J. T. Houghton, Y. Ding, D. J. Griggs, M. Noguer, P. J. van der Linden
483 and D. Xiaosu), New York, NY: Cambridge University Press.
484 Jacobson, M. Z. (2001), Global direct radiative forcing due to multicomponent anthropogenic and
485 natural aerosols, J. Geophys. Res ., 106(D2), 1551-1568.
486 Jaeglé, L., Quinn, P. K., Bates, T. S., Alexander, B., and Lin, J.-T.: Global distribution of sea salt
487 aerosols: new constraints from insitu and remote sensing observations, Atmos. Chem. Phys.,
488 11, 3137–3157, doi:10.5194/acp-11-3137-2011, 2011.
489 Kogan, Yefim L., David B. Mechem, Kityan Choi, Effects of Sea-Salt Aerosols on Precipitation
490 in Simulations of Shallow Cumulus, https://doi.org/10.1175/JAS-D-11-031.1, 2012.

491 Keene W. C., Psxenny A. A. P., Galloway J. N. and Hawley M. E. (1986) Seasalt corrections and
492 interpretation of constituent ratios in marine precipitation. J. Geophys. RES. 91,6647-6658.
493 Kishcha, P., Nickovic, S., Starobinetes, B., di Sarra, A., Udisti, R., Becagli, S., Sferlazzo, D.,
494 Bommarito, C., Alpert, P., 2011. Sea-salt aerosol forecasts compared with daily
495 measurements at the island of Lampedusa (Central Mediterranean). Atmospheric Research
496 100, 28-35.
497 Lawler, M. J., Sander, R., Carpenter, L. J., Lee, J. D., von Glasow, R., Sommariva, R., and
498 Saltzman, E. S.: HOCl and Cl2 observations in marine air, Atmos. Chem. Phys., 11, 7617-
499 7628, https://doi.org/10.5194/acp-11-7617-2011, 2011.
500 Lebsock MD, L'Ecuyer TS, Stephens GL (2011) Detecting the ratio of rain and cloud water in
501 low-latitude shallow marine clouds. J Appl Meteorol Climatol 50:419-432.
502 https://doi.org/10.1175/2010JAMC2494.1.
503 Levy, R. C., Mattoo, S., Munchak, L. A., Remer, L. A., Sayer, A. M., Patadia, F., and Hsu, N. C.:
504 The Collection 6 MODIS aerosol products over land and ocean, Atmos. Meas. Tech., 6,
505 2989-3034, https://doi.org/10.5194/amt-6-2989-2013, 2013.
506 Lewis, E.R., Schwartz, S.E., 2004. Sea salt aerosol production: mechanisms, methods,
507 measurements and models - a critical review. Geophysical Monograph, vol. 152. Print
508 ISBN:9780875904177 |Online ISBN:9781118666050 |DOI:10.1029/GM152, American
509 Geophysical Union, Washington, DC.
510 May, N. W., Quinn, P. K., McNamara, S. M., and Pratt, K. A.: Multiyear study of the dependence
511 of sea salt aerosol on wind speed and sea ice conditions in the coastal Arctic, J. Geophys.
512 Res.-Atmos., 121, 9208–9219, https://doi.org/10.1002/2016JD025273, 2016.
513 McNaughton, C. S., Clarke, A. D., Howell, S. G., Pinkerton, M., Anderson, B., Thornhill, L.,
514 Hudgins, C., Winstead, E., Dibb, J. E., Scheuer, E., and Maring, H.: Results from the DC-8
515 Inlet Characterization Experiment (DICE): Airborne Versus Surface Sampling of Mineral
516 Dust and Sea Salt Aerosols, Aerosol. Sci. Tech., 41, 136–159, 2007.

517 Murphy, D. M., Anderson, J. R., Quinn, P. K., McInnes, L. M., Brechtel, F. J., Kreidenweis, S.
518 M., Middlebrook, A. M., Posfai, M., Thomson, D. S., and Buseck, P. R.: Influence of sea-
519 salt on aerosol radiative properties in the Southern Ocean marine boundary layer, Nature,
520 392, 62–65, 1998.
521 Neumann, D., Matthias, V., Bieser, J., Aulinger, A., and Quante, M.: A comparison of sea salt
522 emission parameterizations in north-western Europe using a chemistry transport model
523 setup, Atmos. Chem. Phys., 16, 9905–9933, doi:10.5194/acp-16-9905-2016, 2016.
524 Pierce, J. R., and P. J. Adams (2006), Global evaluation of CCN formation by direct emission of
525 sea salt and growth of ultrafine sea salt, J. Geophys. Res., 111, D06203,
526 doi:10.1029/2005JD006186.
527 PK Quinn and TS Bates, Ocean-Derived Aerosol and Its Climate Impacts, 5.12, Published by
528 Elsevier Ltd., 2013.
529 Quinn, P. K., Coffman, D. J., Johnson, J. E., Upchurch, L. M., & Bates, T. S. (2017). Small
530 fraction of marine cloud condensation nuclei made up of sea spray aerosol. Nature
531 Geoscience, 10(9), 674–679.
532 Randles, C. A., Russell, L. M., and Ramaswamy, V.: Hygroscopic and optical properties of
533 organic sea salt aerosol and consequences for climate forcing, Geophys. Res. Lett., 31, L16
534 108, doi:10.1029/2004GL020628, 2004.
535 Randles, C. A., da Silva, A. M., Buchard, V., Colarco, P. R., Darmenov, A., Govindaraju, R.,
536 Smirnov, A., Holben, B., Ferrare, R., Hair, J., Shinozuka, Y., and Flynn, C. J.: The
537 MERRA-2 Aerosol Reanalysis, 1980-onward, Part I: System Description and Data
538 Assimilation Evaluation, J. Climate, 30, 6823–6850, https://doi.org/10.1175/jcli-d-16-
539 0609.1, 2017.
540 Rhodes, R. H., Yang, X., Wolff, E. W., McConnell, J. R., and Frey, M. M.: Sea ice as a source of
541 sea salt aerosol to Greenland ice cores: a model-based study, Atmos. Chem. Phys., 17,
542 9417–9433, https://doi.org/10.5194/acp-17-9417-2017, 2017.

543 Rienecker, M. M., Suarez, M. J., Gelaro, R., Todling, R., Bacmeister, J., Liu, E., Bosilovich, M.
544 G., Schubert, S. D., Takacs, L.,Kim, G. K., Bloom, S., Chen, J., Collins, D., Conaty, A., da
545 Silva, A., Gu, W., Joiner, J., Koster, R. D., Lucchesi, Andrea Molod, A., Owens, T.,
546 Pawson. S., Pegion, P., Redder, C. R., Reichle, R., Robertson, F. R., Ruddick, A. G.,
547 Sienkiewicz, M., and Woollen, J.: MERRA: NASA's Modern-Era Retrospective Analysis
548 for Research and Applications, J. Climate, 24, 3624–3648, 2011.
549 Salter, M. E., P. Zieger, J. C. Acosta Navarro, H. Grythe, A. Kirkevåg, B. Rosati, I. Riipinen, and
550 E. D. Nilsson (2015), An empirically derived inorganic sea spray source function
551 incorporating sea surface temperature, Atmos. Chem. Phys., 15(19), 11,047–11,066,
552 doi:10.5194/acp-15-11047-2015.
553 Smirnov, A., M. Petrenko, C. Ichoku, and B. Holben. 2017. "Maritime Aerosol Network optical
554 depth measurements and comparison with satellite retrievals from various different sensors."
555 Remote Sensing of Clouds and the Atmosphere XXII, [10.1117/12.2277113].
556 Spada, M., Jorba, O., Pérez García-Pando, C., Janjic, Z., and Baldasano, J. M.: Modeling and
557 evaluation of the global sea-salt aerosol distribution: sensitivity to size-resolved and sea-
558 surface temperature dependent emission schemes, Atmos. Chem. Phys., 13, 11735-11755,
559 https://doi.org/10.5194/acp-13-11735-2013, 2013.
560 Spada, M., Jorba, O., Pérez García-Pando, C., Janjic, Z., and Baldasano, J. M.: On the evaluation
561 of global sea-salt aerosol models at coastal/orographic sites, Atmos. Environ., 101, 41–48,
562 https://doi.org/10.1016/j.atmosenv.2014.11.019, 2015
563 Takemura, T., Nakajima, T., Dubovik, O., Holben, B. N., and Kinne, S.: Single-scattering albedo
564 and radiative forcing of various aerosol species with a global three-dimensional model, J.
565 Climate, 15(4), 333–352, 2002
566 Textor, C., Schulz, M., Guibert, S., Kinne, S., Balkanski, Y., Bauer, S., Berntsen, T., Berglen, T.,
567 Boucher, O., Chin, M., Dentener, F., Diehl, T., Easter, R., Feichter, H., Fillmore, D., Ghan,
568 S., Ginoux, P., Gong, S., Grini, A., Hendricks, J., Horowitz, L., Huang, P., Isaksen, I.,

Iversen, I., Kloster, S., Koch, D., Kirkevåg, A., Kristjansson, J. E., Krol, M., Lauer, A., Lamarque, J. F., Liu, X., Montanaro, V., Myhre, G., Penner, J., Pitari, G., Reddy, S., Seland, Ø., Stier, P., Takemura, T., and Tie, X.: Analysis and quantification of the diversities of aerosol life cycles within AeroCom, Atmos. Chem. Phys., 6, 1777–1813, https://doi.org/10.5194/acp-6-1777-2006, 2006.

Tsyro, S., W. Aas, J. Soares, M. Sofiev, H. Berge, and G. Spindler, Modelling of sea salt concentrations over Europe: key uncertainties and comparison with observations, Atmos. Chem. Phys., 11, 10367–10388, 2011, www.atmos-chem-phys.net/11/10367/2011/, doi:10.5194/acp-11-10367-2011.

Wilson, T. R. S., Salinity and the major elements of sea water, in Chemical Oceanography, vol. 1, 2nd ed., edited by J.P. Riley and G. Skirrow, pp. 365-413, Academic, Orlando, Fla., 1975.

Witek, M. L., P. J. Flatau, P. K. Quinn, and D. L. Westphal, 2007: Global sea-salt modeling: Results and validation against multicampaign shipboard measurements. J. Geophys. Res., 112, D08215, doi:10.1029/2006JD007779.

Wood, R., 2012. Stratocumulus clouds. Month. Weath. Rev. 140, 2373–2423.

Zhou, X., Kollias, P., & Lewis, E. R. (2015). Clouds, precipitation, and marine boundary layer structure during the MAGIC field campaign. Journal of Climate, 28(6), 2420–2442. https://doi.org/10.1175/JCLI-D-14-00320.1.

Atmos. Chem. Phys. Discuss., https://doi.org/10.5194/acp-2019-18
Manuscript under review for journal Atmos. Chem. Phys.
Discussion started: 28 January 2019

Atmospheric Chemistry and Physics Discussions

Table 1a. GEOS sea salt budget analysis for the particles up to 3 μm in dry diameters using the three emission algorithms on annual basis from July 2016 to June 2017

	Emi1	Emi2	Emi3	
Emission (Tg/yr)	408.8	615.6	515.2	
Burden (Tg)	1.21	1.88	1.63	
Lifetime (days)	1.08	1.12	1.16	
Surf concentration (μg/kg)	2.5	3.9	3.2	
Dry deposition (Tg/yr)	82.4	127.0	103.1	
Sedimentation (Tg/yr)	60.7	88.7	61.1	
Kdry ($days^{-1}$)	1.37	1.32	1.17	
Wet deposition (Tg/yr)	123.8	181.9	140.3	
SV deposition (Tg/yr)	142.2	218.8	211.8	
Kwet ($days^{-1}$)	0.45	0.43	0.44	

Table 1b. Similar to Table 1a but for all particle size range

	Emi1	Emi2	Emi3	AeroCom
Emission (Tg/yr)	3185.7	4797.6	4015.5	2190-117949
Burden (Tg)	4.79	7.55	6.80	3.4-18.2
Lifetime (days)	0.55	0.57	0.62	0.03-1.59
Surf concentration (μg/kg)	12.2	18.9	16.5	
Dry deposition (Tg/yr)	353.6	547.9	460.9	
Sedimentation (Tg/yr)	2049.0	3064.3	2458.2	
Kdry ($days^{-1}$)	1.37	1.32	1.17	0.06-2.94
Wet deposition (Tg/yr)	278.9	417.0	354.7	
SV deposition (Tg/yr)	505.1	771.1	746.1	
Kwet ($days^{-1}$)	0.45	0.43	0.44	0.11-2.45
$SSAOD_{550nm}$	0.0206	0.0318	0.0269	0.003-0.067

Table 2. Sea salt mass extinction efficient (MEE) for PALMS and GEOS and the ratio of MEEs between GEOS and PALMS in three vertical layers and in the whole atmosphere at RH 45%

	PALMS (m2/kg)	GEOS (m2/kg)	R(GEOS/PALMS) %
0 – 1.5 KM	2636.87	1618.09	61.4
1.5 – 6 KM	2089.97	1671.61	80.0
>6 KM	1891.07	1786.24	94.5
all	2203.67	1679.36	76.2

615 **Figure Captions**

616 **Figure 1**. AToM1 (top) and AToM2 (bottom) flight track sorted out for each flight day.

617

618 **Figure 2a**. Scattering plot of sea salt between GEOS and PALMS (magenta) and between
619 GEOS and SAGA (blue) in ATom1 (symbol +) and ATom2 (symbol ◇) for all flight
620 measurements within 1.5 km atmospheric thickness above ocean surface. The SAGA
621 samples are filtered out when dust signal is significant. The GEOS sea salt shown here
622 are cut at 3 μm in dry diameters. Both GEOS and PALMS data are then sampled using
623 SAGA measurement time frequency.

624

625 **Figure 2b**. Similar to Figure 2a with the samples contaminated by clouds are further
626 excluded using CAPS cloud indicator.

627
628 **Figure 3**. Sea salt (Dp < 3 μm) vertical profiles from GEOS simulation and PALMS
629 measurement along ATom1 and 2 flight tracks in 5 latitudinal bands over Pacific and
630 Atlantic oceans. The latitudinal bands are marked by dot grey lines in Figure 1.

631

632 **Figure 4**. Total aerosol AOD in 201608 (left column) and 201702 (right column) from
633 MODIS (top) and GEOS (middle). The bottom panel shows the mass fraction of sea salt
634 relative to the total aerosol simulated by GEOS.

635

636 **Figure 5**. Total AOD measured by MAN cruise occurred during 201607 to 201706 (5a)
637 and simulated by GEOS but sampled with MAN measurement (5b). 5c shows total AOD

638 scattering plot between MAN and GEOS and the purple color is for the data over
639 Southern Ocean shown inside the boxes in Figure 5b.
640
641 **Figure 6**. Percentage distribution of sea salt mass over the first three bins normalized to
642 the total sea salt with particle wet diameter up to ~5 μm at RH 45%. The normalized SS
643 mass weighting distribution is sorted over three vertical layers and for ATom1 and
644 ATom2, respectively.
645
646 **Figure 7**. Atmospheric RH vertical profiles from GEOS simulation and ATom
647 measurement along ATom1 and 2 flight tracks in 5 latitudinal bands over Pacific and
648 Atlantic oceans.
649
650
651
652
653
654
655

Atmos. Chem. Phys. Discuss., https://doi.org/10.5194/acp-2019-18
Manuscript under review for journal Atmos. Chem. Phys.
Discussion started: 28 January 2019

Atmospheric Chemistry and Physics Discussions

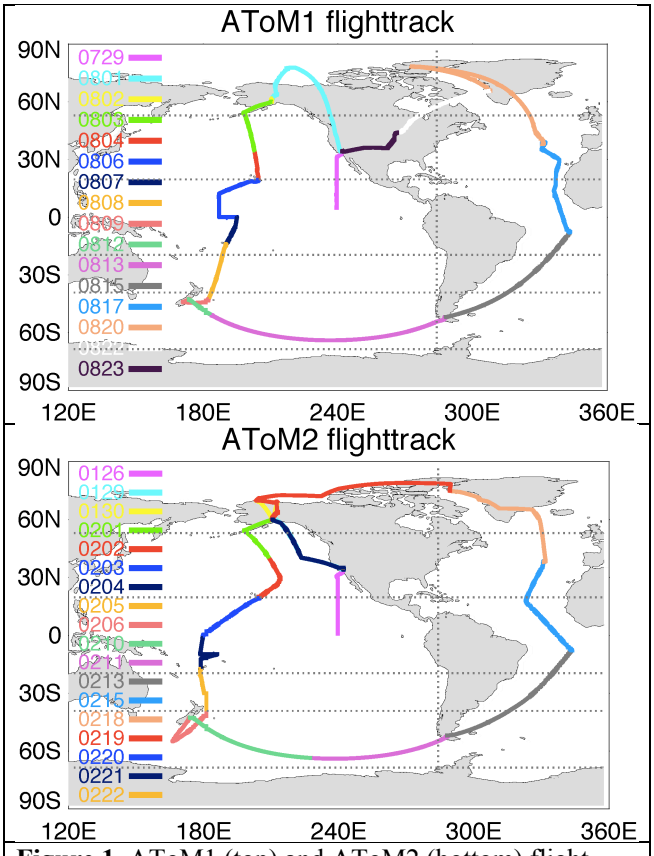

Figure 1. AToM1 (top) and AToM2 (bottom) flight track sorted out for each flight day.

Atmos. Chem. Phys. Discuss., https://doi.org/10.5194/acp-2019-18
Manuscript under review for journal Atmos. Chem. Phys.
Discussion started: 28 January 2019

Atmospheric Chemistry and Physics Discussions

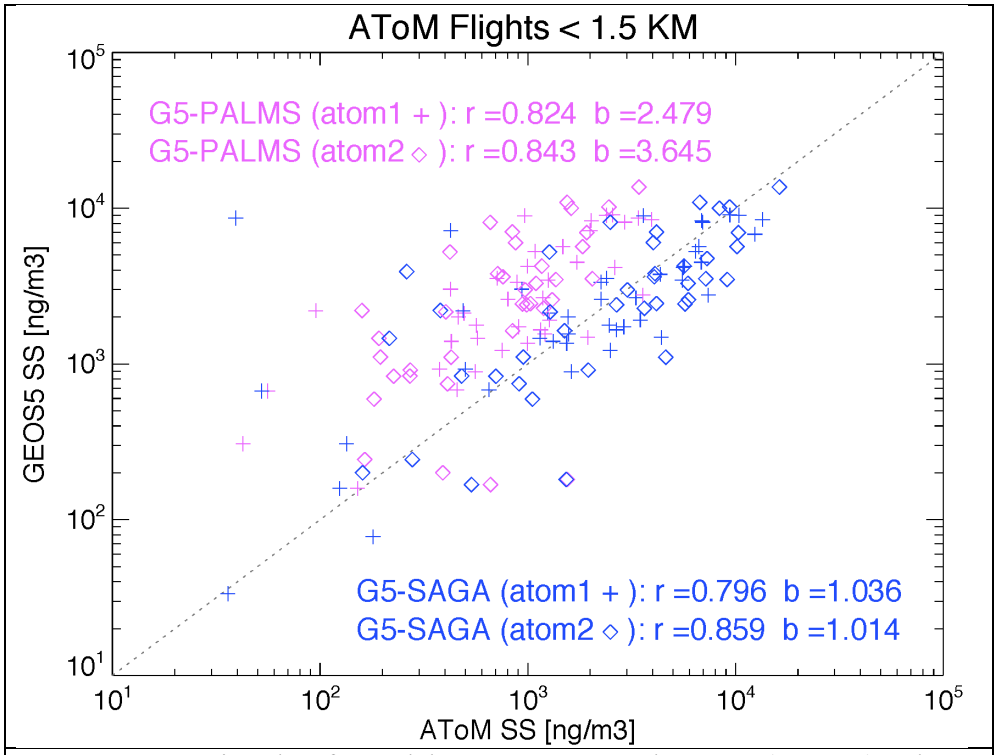

Figure 2a. Scattering plot of sea salt between GEOS5 and PALMS (magenta) and between GEOS5 and SAGA (blue) in ATom1 (symbol +) and ATom2 (symbol ◇) for all flight measurements within 1.5 km atmospheric thickness above ocean surface. The SAGA samples are filtered out when dust signal is significant. The GEOS5 sea salt shown here are cut at 3 μm in dry diameters. Both GEOS5 and PALMS data are then sampled using SAGA measurement time frequency.

674
675
676
677

Atmos. Chem. Phys. Discuss., https://doi.org/10.5194/acp-2019-18
Manuscript under review for journal Atmos. Chem. Phys.
Discussion started: 28 January 2019

Atmospheric Chemistry and Physics Discussions

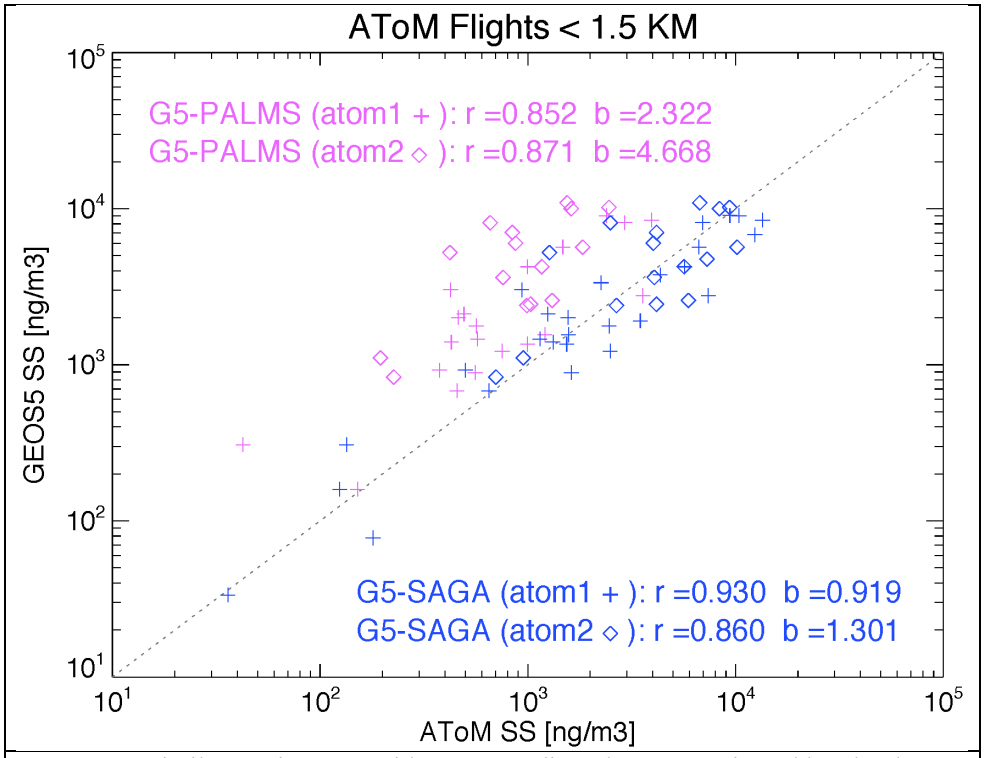

Figure 2b. Similar to Figure 2a with SAGA sodium data contaminated by clouds are further excluded using CAPS cloud indicator.

Atmos. Chem. Phys. Discuss., https://doi.org/10.5194/acp-2019-18
Manuscript under review for journal Atmos. Chem. Phys.
Discussion started: 28 January 2019

Atmospheric Chemistry and Physics Discussions

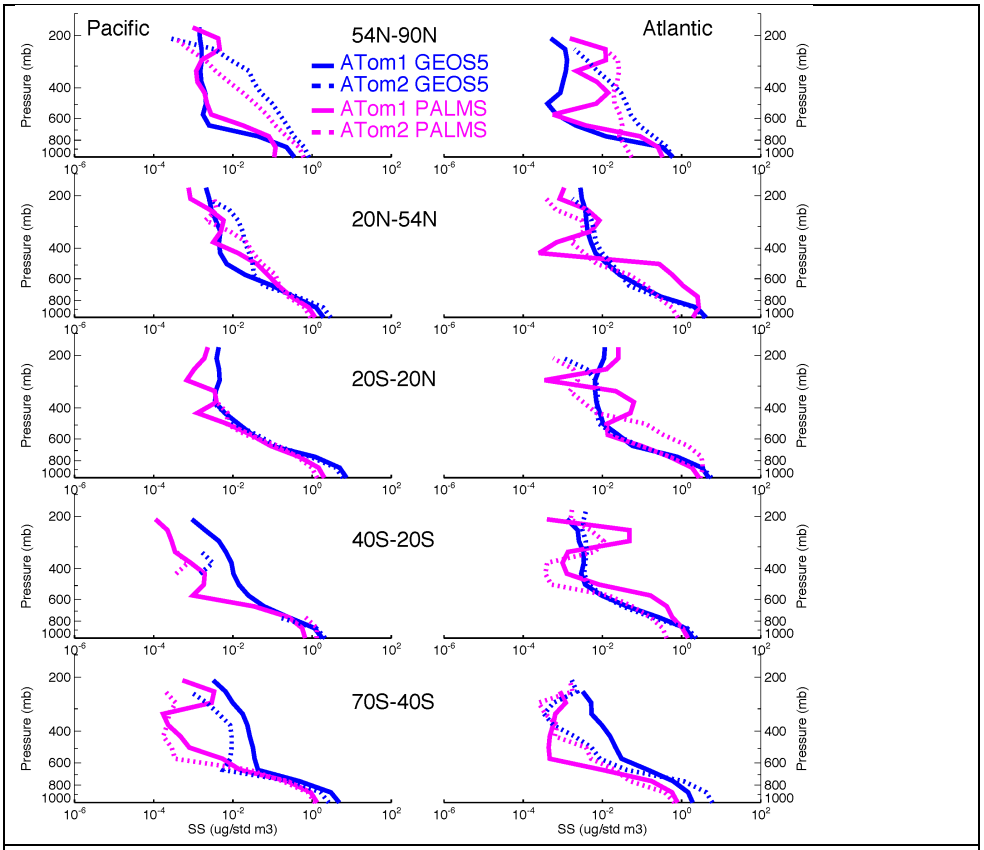

Figure 3. Sea salt (Dp < 3 μm) vertical profiles from GEOS5 simulation and PALMS measurement along ATom1 and 2 flight tracks in 5 latitudinal bands over Pacific and Atlantic oceans. The latitudinal bands are marked by dot grey lines in Figure 1.

Atmos. Chem. Phys. Discuss., https://doi.org/10.5194/acp-2019-18
Manuscript under review for journal Atmos. Chem. Phys.
Discussion started: 28 January 2019

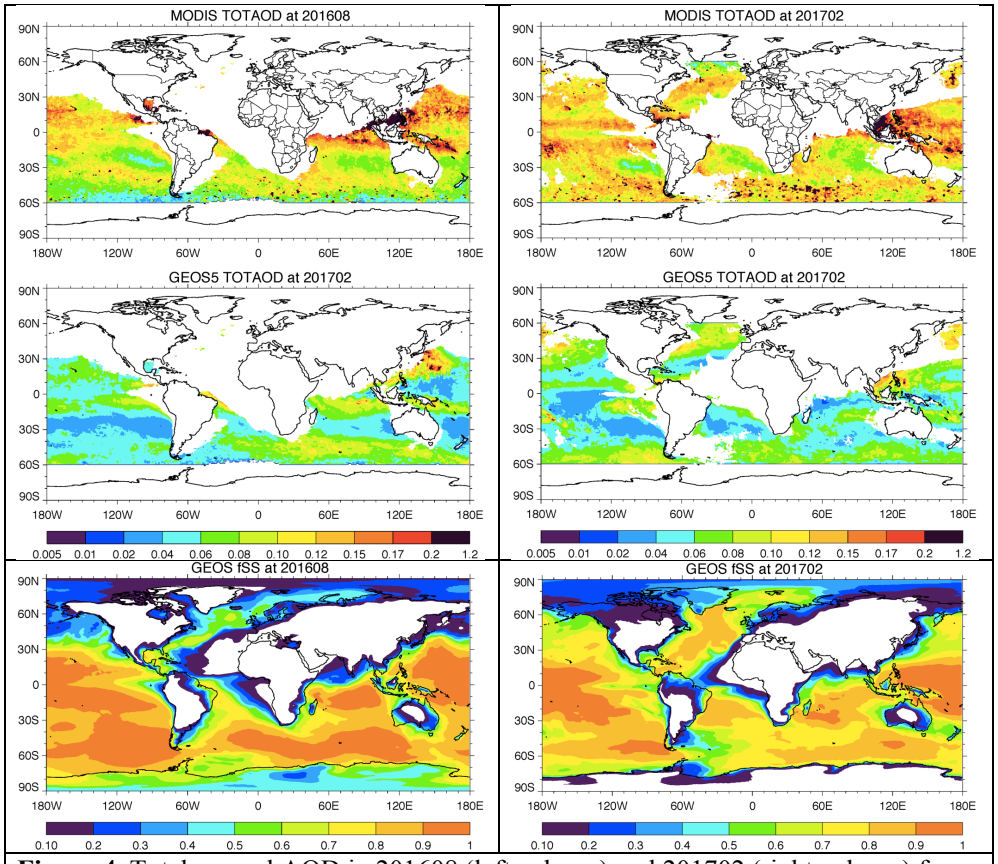

Figure 4. Total aerosol AOD in 201608 (left column) and 201702 (right column) from MODIS (top) and GEOS5 (middle) over oceans where fraction of sea salt mass simulated by GEOS (bottom panel) is larger than 0.7.

Atmos. Chem. Phys. Discuss., https://doi.org/10.5194/acp-2019-18
Manuscript under review for journal Atmos. Chem. Phys.
Discussion started: 28 January 2019

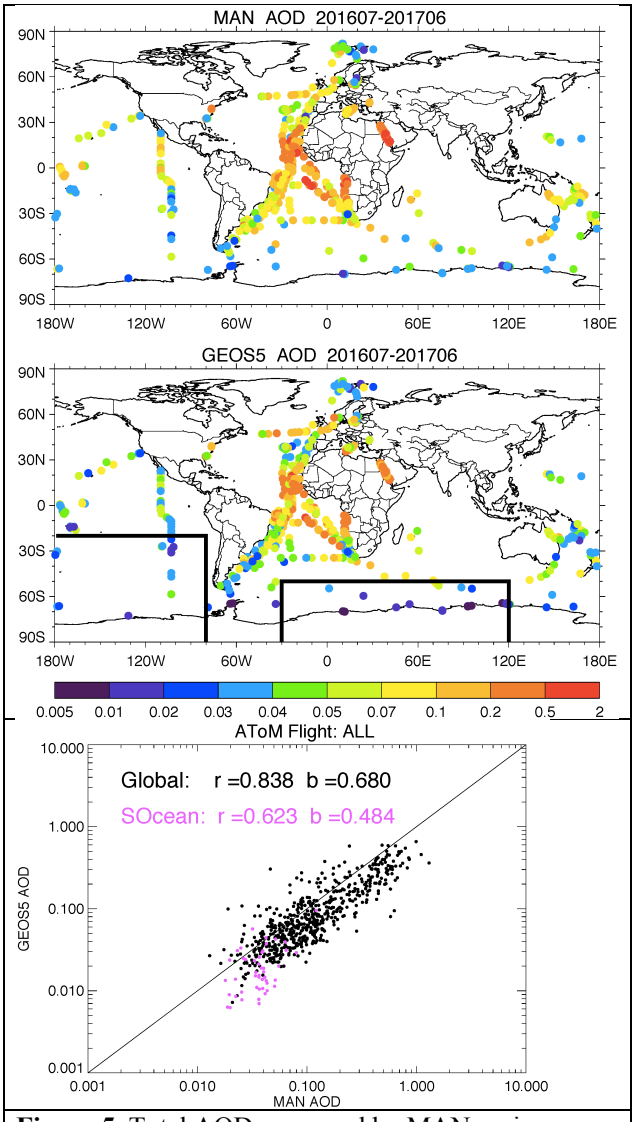

Figure 5. Total AOD measured by MAN cruise occurred during 201607 to 201706 (5a) and simulated by GEOS5 but sampled with MAN measurement (5b). 5c shows total AOD scattering plot between MAN and GEOS and the purple color is for the data over Southern Ocean shown inside the boxes in Figure 5b.

Atmos. Chem. Phys. Discuss., https://doi.org/10.5194/acp-2019-18
Manuscript under review for journal Atmos. Chem. Phys.
Discussion started: 28 January 2019

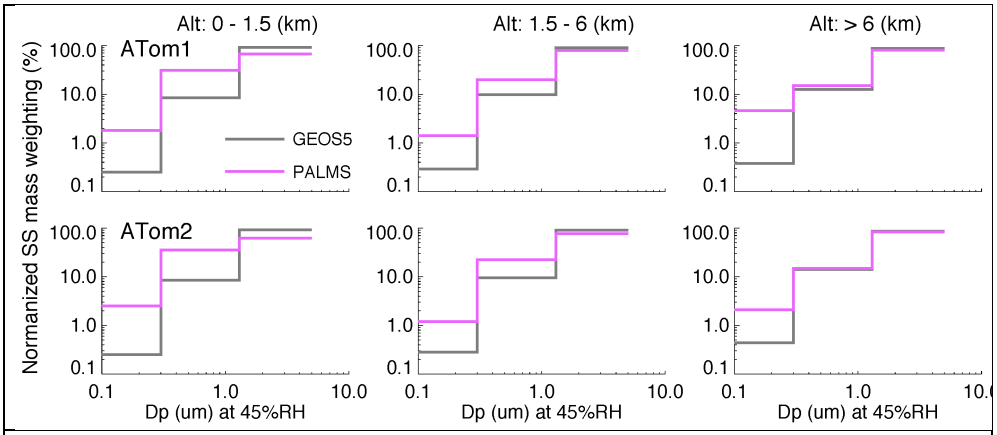

Figure 6. Percentage distribution of sea salt mass over the first three bins normalized to the total sea salt with particle wet diameter up to ~5 μm at RH 45%. The normalized SS mass weighting distribution is sorted over three vertical layers and for ATom1 and ATom2, respectively.

Atmos. Chem. Phys. Discuss., https://doi.org/10.5194/acp-2019-18
Manuscript under review for journal Atmos. Chem. Phys.
Discussion started: 28 January 2019

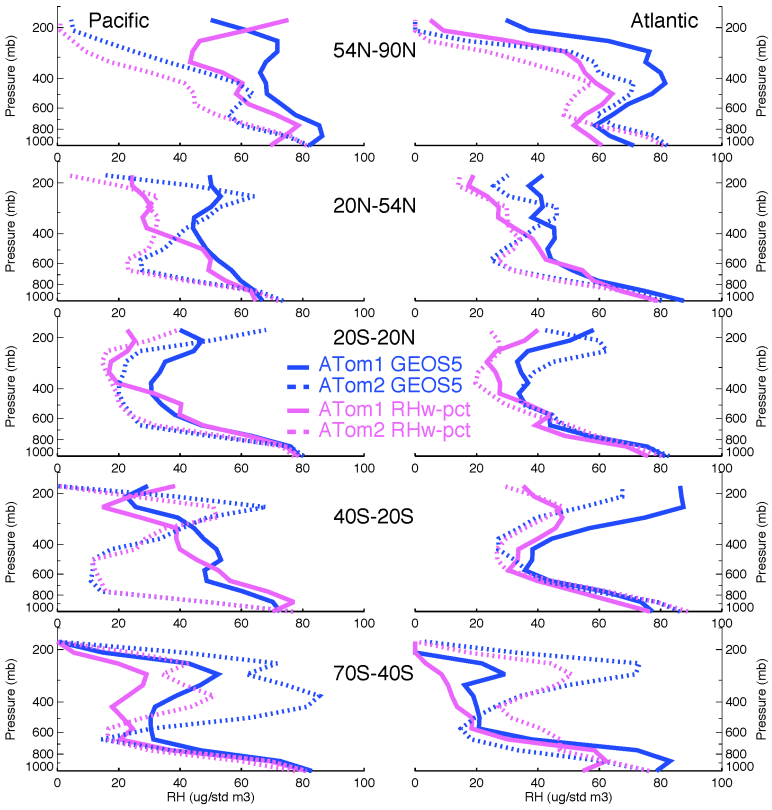

Figure 7. Atmospheric RH vertical profiles from GEOS5 simulation and ATom measurement along ATom1 and 2 flight tracks in 5 latitudinal bands over Pacific and Atlantic oceans.

727